

RESEARCH ARTICLE | *Nutrient Sensing, Nutrition, and Metabolism*

Intestine-specific deletion of metal transporter *Zip14* (*Slc39a14*) causes brain manganese overload and locomotor defects of manganism

Tolunay B. Aydemir,¹ Trista L. Thorn,¹ Courtney H. Ruggiero,² Marjory Pompilus,³ Marcelo Febo,³ and Robert J. Cousins^{2,4}

¹Division of Nutritional Sciences, Cornell University, Ithaca, New York; ²Food Science and Human Nutrition Department, Center for Nutritional Sciences, College of Agricultural and Life Sciences, University of Florida, Gainesville, Florida;

³Department of Psychiatry, McKnight Brain Institute, University of Florida, Gainesville, Florida; and ⁴Department of Biochemistry and Molecular Biology, College of Medicine, University of Florida, Gainesville, Florida

Submitted 1 October 2019; accepted in final form 28 January 2020

Aydemir TB, Thorn TL, Ruggiero CH, Pompilus M, Febo M, Cousins RJ. Intestine-specific deletion of metal transporter *Zip14* (*Slc39a14*) causes brain manganese overload and locomotor defects of manganism. *Am J Physiol Gastrointest Liver Physiol* 318: G673–G681, 2020. First published January 31, 2020; doi:10.1152/ajpgi.00301.2019.—Impaired manganese (Mn) homeostasis can result in excess Mn accumulation in specific brain regions and neuropathology. Maintaining Mn homeostasis and detoxification is dependent on effective Mn elimination. Specific metal transporters control Mn homeostasis. Human carriers of mutations in the metal transporter ZIP14 and whole body *Zip14*-knockout (WB-KO) mice display similar phenotypes, including spontaneous systemic and brain Mn overload and motor dysfunction. Initially, it was believed that Mn accumulation due to ZIP14 mutations was caused by impaired hepatobiliary Mn elimination. However, liver-specific *Zip14*-KO mice did not show systemic Mn accumulation or motor deficits. ZIP14 is highly expressed in the small intestine and is localized to the basolateral surface of enterocytes. Thus, we hypothesized that basolaterally localized ZIP14 in enterocytes provides another route for the elimination of Mn. Using wild-type and intestine-specific *Zip14*-KO (I-KO) mice, we have shown that ablation of intestinal *Zip14* is sufficient to cause systemic and brain Mn accumulation. The lack of intestinal ZIP14-mediated Mn excretion was compensated for by the hepatobiliary system; however, it was not sufficient to maintain Mn homeostasis. When supplemented with extra dietary Mn, I-KO mice displayed some motor dysfunctions and brain Mn accumulation based on both MRI imaging and chemical analysis, thus demonstrating the importance of intestinal ZIP14 as a route of Mn excretion. A defect in intestinal *Zip14* expression likely could contribute to the Parkinson-like Mn accumulation of manganism.

NEW & NOTEWORTHY Mn-induced parkinsonism is recognized as rising in frequency because of both environmental factors and genetic vulnerability; yet currently, there is no cure. We provide evidence in an integrative animal model that basolaterally localized ZIP14 regulates Mn excretion and detoxification and that deletion of intestinal ZIP14 leads to systemic and brain Mn accumulation, providing robust evidence for the indispensable role of intestinal ZIP14 in Mn excretion.

detoxification; manganism; neuroinflammation; parkinsonism; transport

INTRODUCTION

Accumulation of manganese (Mn) in the brain of rodents produces a neurodegenerative disease (manganism) with signatures that are similar to those in humans with Parkinson's disease-like symptoms (parkinsonism) and dystonia (26, 27, 30, 32). Recently, considerable attention has been given to Mn-induced neurodegeneration and parkinsonism in humans (1, 10, 15, 22, 24). Potential causes of excess Mn accumulation include occupational exposure and contaminated drinking water (36), vegetarian diets and overconsumption of Mn-containing dietary supplements (12), chronic liver disease (28, 34), and abuse of amphetamine-like drugs (13). The deleterious effects of Mn exposure on human health are amplified by the increased atmospheric levels of Mn from exhaust emissions (8). These numerous potential routes of chronic Mn exposure, coupled with increased lifespans of humans, have increased the prevalence of Mn-related neurodegenerative disease worldwide (9, 11, 18, 29).

Mutations in the human metal transporter genes *ZNT10*, *ZIP8*, and *ZIP14* impair Mn homeostasis (6, 19, 20, 25, 28, 35). Mutations in the solute-carrier (*SLC*) *39A14* gene encoding the ZIP14 transporter were found in patients with childhood-onset parkinsonism and dystonia with systemic and brain Mn accumulation (35). Since that discovery, there have been a number of case reports of similar symptoms in humans with ZIP14 mutations (17, 23, 31, 38). Whole body *Zip14* KO mice display phenotypes similar to those of human carriers of ZIP14 mutations, including spontaneous systemic and brain Mn overload, specifically in the globus pallidus, and motor dysfunction (3). Hepatic Mn uptake and intestinal Mn elimination were also impaired in whole body *Zip14*-KO mice compared with wild-type (WT) mice.

Mn elimination is crucial for maintaining homeostasis and detoxification; however, very little is known about how it is regulated. ZIP14 is highly expressed in the small intestine and liver at steady state compared with other tissues (21). The main route of Mn excretion is via bile (15). Thus, Mn accumulation caused by ZIP14 mutations in humans was initially believed to be associated with impaired hepatobiliary Mn elimination (35). However, liver-specific *Zip14*-KO mice do not show systemic Mn accumulation or motor deficits (37), suggesting that Mn is eliminated by an alternative route. In enterocytes, ZIP14 has a basolateral orientation (BL) (3, 14). We have previously shown

Address for reprint requests and other correspondence: T. B. Aydemir, Div. of Nutritional Sciences, Cornell Univ., Ithaca, NY 14853 (e-mail: tb536@cornell.edu).

that when administered subcutaneously, ^{54}Mn levels were lower in intestinal tissue and the intestinal contents of whole body *Zip14*-KO (WB-KO) mice compared with WT mice, suggesting that systemic Mn elimination is less effective in the absence of ZIP14 (3). Thus, our working hypothesis centers on BL-localized ZIP14 in enterocytes providing a route for elimination of Mn. Using comparisons between whole body and intestine-specific *Zip14*-KO mice, we demonstrate here that deletion of intestinal *Zip14* is sufficient to cause systemic Mn overload and that intestinal ZIP14 is a significant contributor to Mn homeostasis.

MATERIALS AND METHODS

Mice

After being weaned, the mice were fed ad libitum a commercial chow diet that contained 93 mg Mn/kg (Harlan 7012) and tap water, and the mice were maintained on a 12/12 h light/dark cycle. Mice were used as young adults (8–16 wk of age). Both sexes were included in all experiments. Euthanasia was through exsanguination by cardiac puncture under isoflurane anesthesia. Protocols were approved by the both Cornell University and University of Florida Institutional Animal Care and Use Committees.

Whole body *Zip14*-KO mice. The design and validation of the conventional *Zip14*-KO (*Zip14*^{-/-}) (WB-KO) murine strain has been described previously (2, 4). The breeding colony has been maintained with backcrosses of the C57BL/6;129S5 background. The mice used in these experiments were of the F12 generation or later.

Intestine-specific *Zip14*-KO mice. Floxed *Zip14* mice on the 129Sv background were generated using targeting of introns 4 and 8. Founder *Zip14*^{fllox/+} mice were bred to obtain *Zip14*^{fllox/fllox} (*Zip14*^{fl/fl}) mice at the University of Florida. Following genotype confirmation, *Zip14*^{fl/fl} mice were crossed with B6.Cg-Tg(Vil1-cre)997Gum/J (Jackson Laboratory, stock no. 004586) mice to create an intestine-specific *Zip14*-KO (I-KO) mouse model with which to evaluate the role of intestinal ZIP14 on Mn absorption and excretion.

Treatments

After 4 h of morning fasting, mice were administered ^{54}Mn either via gavage (5 μCi) or subcutaneous injections (3 μCi). The mice were euthanized 4 h later via cardiac puncture to collect blood and tissues. The entire excised small intestine was perfused with a metal chelating buffer (10 mM EDTA, 10 mM HEPES, and 0.9% NaCl₂). The ^{54}Mn content of tissues was measured by gamma-ray solid scintillation spectrometry and normalized by tissue weight.

Manganese exposure. Either control or Mn-supplemented (2 mg Mn/L as MnCl₂) water was provided to the mice for 1 mo. We chose to supplement Mn via the drinking water to maintain a relatively constant consumption of the diet.

Genotyping

Genomic DNA was extracted from mouse tail biopsies using extraction buffer (25 mM NaOH/0.2 mM EDTA) and incubation at 98°C for 45 min (33). The genotyping protocol for whole body *Zip14*-KO mice has been presented previously (2). The following primer sets were used for genotyping *Zip14*^{fl/fl} and villin-cre+ mice: flox forward 5'-AGT GGC CAT GGT AGT TCC TG-3', flox reverse 5'-CCT GGT GCC TGC ATA TTC TC-3' and cre reverse 5'-CAT GTC CAT CAG GTT CTT GC-3', cre forward 5'-TTC TCC TCT AGG CTC GTC CA-3', internal positive control forward 5'-CTA GGC CAC AGA ATT GAA AGA TCT-3', internal positive control reverse 5'-GTA GGT GGA AAT TCT AGC ATC ATC C-3', respectively.

Metal Assays

To measure Mn concentrations, weighed aliquots of tissue were digested at 95°C for at least 3 h in HNO₃. Whole blood (500 μL) was dried and then digested for 24 h in HNO₃. The entire excised small intestine was perfused with a metal chelating buffer (10 mM EDTA, 10 mM HEPES, and 0.9% NaCl₂) (equal volume/intestine) and then digested for 24 h in HNO₃. Digested samples were diluted in Milli-Q water. Mn was measured by Microwave Plasma-Atomic Emission Spectrometry (MP-AES) using 403.076 nm for emission detection. Normalization was to tissue or body weight (intestinal contents).

Reactive Oxygen Species Assay

Whole brain tissues were homogenized in lysis buffer (250 mM sucrose, 20 mM HEPES-NaOH, pH 7.5, 10 mM KCl, 1.5 mM MgCl₂, 1 mM EDTA, 1 mM EGTA) that supplemented with protease inhibitors. Following centrifugation at 800 g for 10 min, supernatants were incubated with 2,7-dichlorodihydrofluorescein diacetate (Cayman, 4091–99–0) at 37°C for 1 h. The fluorescent signal was measured at 502/523 nm.

Western Blot

Tissue was homogenized in lysis buffer with protease and phosphatase inhibitors (Thermo Scientific and AGScientific) added along with the PMSF (Sigma-Aldrich) using the Bullet Blender (Next Advances). Solubilized proteins were separated by 10% SDS-PAGE. Visualization was by chemiluminescence (SuperSignal, Thermo Fisher) and digital imaging (Protein Simple). Rabbit anti-mouse ZIP14 antibody was custom made by Genscript. Antibodies for GAPDH and actin were obtained from Cell Signaling.

Quantitative PCR Analyses

Tissues were homogenized in TRIzol reagent using the Bullet Blender homogenizer, and RNA was isolated. Total RNA was used to measure relative mRNA abundance by quantitative PCR (qPCR). Primer/probes for inducible nitric oxide synthase, *tnfa*, *il-6*, and GAPDH were purchased from Applied Biosystems.

Motor function. Motor functions were tested in the light phase. All tests were performed as in previous studies (3).

Beam traversal. The beam was constructed of 4 segments of 0.25 m in length. Each segment was of thinner widths (3.5 cm, 2.5 cm, 1.5 cm, and 0.5 cm); the widest segment acted as a loading platform for the mice, and the narrowest end was adjacent to the home cage. After 2 days of training, on the test day, mice were timed over three trials as they traversed from the loading platform and to the home cage.

Pole descent. A pole (0.5 m long, 1 cm in diameter) was placed in the home cage. After 2 days of training, on the test day, the time to descend from the top of the pole to the cage floor was measured.

Fecal output. Mice were transferred from their home cage to a 12 × 20 cm translucent cylinder, and fecal pellets produced over 5 min were counted. The data were generated by using averages of 3 days of trials.

Inverted grid. The mice were placed in the center of a 26 × 38 cm screen with 1 cm²-wide mesh. The screen was inverted for 60 s, and the mice were timed until they released their grip or held on.

Magnetic Resonance Imaging

The MRI scans were collected in a 4.7-T/33-cm horizontal bore magnet (Magnex Scientific) at the Advanced Magnetic Resonance Imaging and Spectroscopy facility in the McKnight Brain Institute of the University of Florida. The MR scanner consisted of a 11.5-cm diameter gradient insert (Resonance Research, Billerica, MA) controlled by a VnmrJ 3.1 software console (Agilent, Palo Alto, CA). A quadrature transmit/receive radiofrequency coil tuned to 200.6 MHz ¹H resonance was used for B1 field excitation and radiofrequency

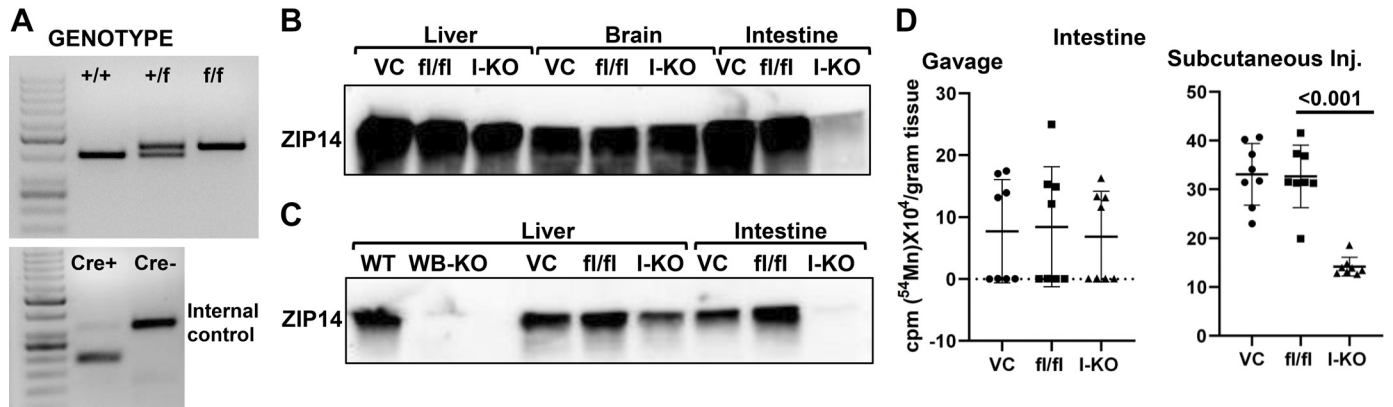


Fig. 1. ^{54}Mn elimination is impaired in intestine-specific *Zip14* knockout (KO) mice. *A*: representative genotype. *B*: representative Western analyses are showing ZIP14 protein levels. ZIP14 protein levels in liver, brain, and intestine of the villin-cre (VC), floxed *Zip14* (fl/fl), and intestine-specific conditional *Zip14*-KO (I-KO) mice. *C*: comparison of ZIP14 protein levels between whole body KO (WB-KO) and intestine-specific *Zip14*-KO mice. *D*: mice were administered ^{54}Mn via either gavage or subcutaneous injection (Inj.). Four hours later, intestinal ^{54}Mn absorption and elimination were measured in floxed *Zip14* (fl/fl) and I-KO mice. Values are means \pm SD; $n = 8$ (both female and male mice were included). Student's *t* test for fl/fl vs. I-KO comparison. WT, wild-type.

signal detection (Animal Imaging Research, Limited Liability Company, Holden, MA). On the scanning day, mice were induced using 3%–4% isoflurane delivered in medical grade air (70% nitrogen, 30% oxygen; air flow rate 1.5 mL/min). The anesthesia was maintained at 1.0%–1.5% isoflurane during MRI scanning. Core body temperature and spontaneous respiratory rates were continuously recorded during MRI scanning (SA Instruments, Stony Brook, NY). Mice were maintained at normal body temperature levels (37°C–38°C) using a warm water recirculation system. The MRI included a multiple repetition time sequence to calculate parametric T1 maps for each group using a fast spin echo sequence with a total of 4 repetition times (TRs) (0.5,

1.08, 2.33, 5.04 s) and echo time of 6.02 ms with the following geometric parameters: $16 \times 16 \text{ mm}^2$ in plane, 14 slices at 0.8-mm thickness per slice, and a 128×128 data matrix (125 μm in-plane resolution).

MRI Postprocessing and Analysis

Whole brain masks were obtained via automated segmentation with three-dimensional pulse-coupled neural networks (PCNN3D) using high-resolution anatomical scans to remove nonbrain voxels. All cropped data were used to create templates for each cohort using

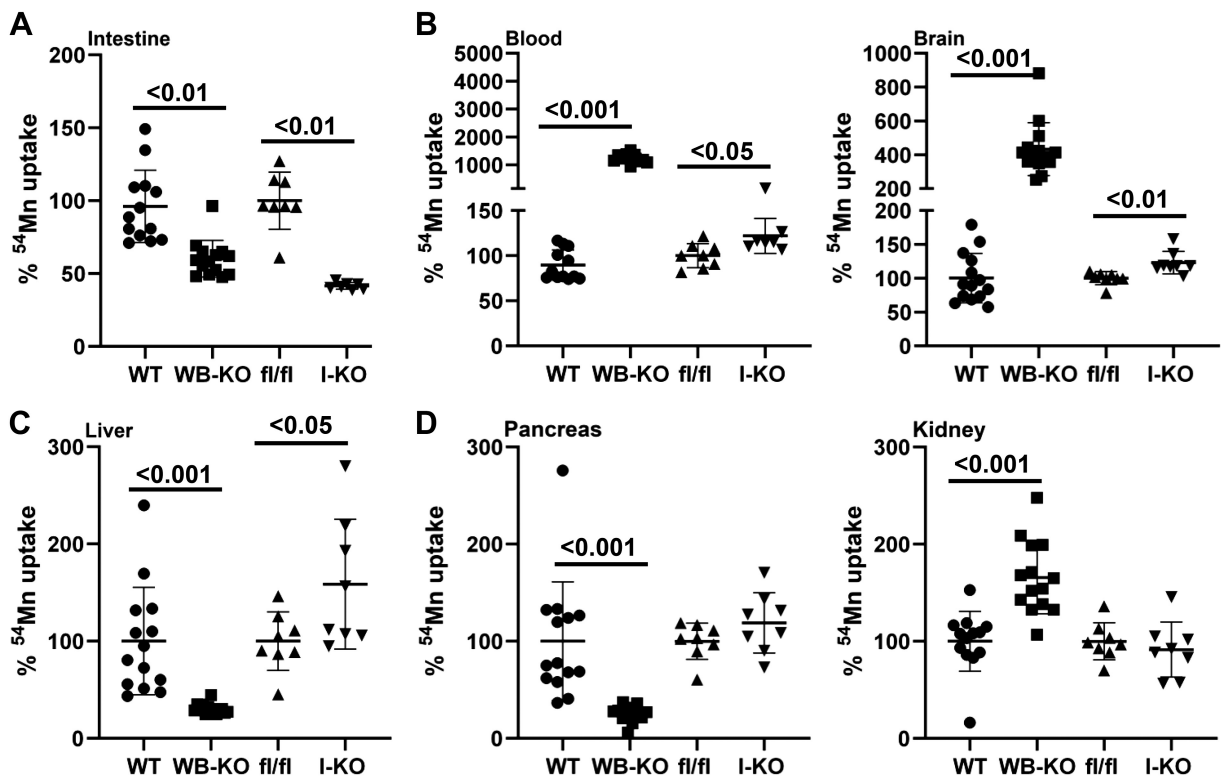


Fig. 2. Comparison of percent ^{54}Mn uptake between whole body (WB) and intestine-specific (I) *Zip14* knockout (KO). Mice were administered ^{54}Mn via subcutaneous injection, and 4 h later radioactivity was measured in intestine (*A*), blood and brain (*B*), liver (*C*), and pancreas and kidney (*D*). Values are reported as means \pm SD; $n = 7$ –14 (both female and male mice were included). Student's *t* test for wild-type (WT) vs. WB-KO and floxed *Zip14* (fl/fl) vs. I-KO comparison.

Advanced Normalization Tools (<http://stnava.github.io/ANTs/>). The templates were then registered to an atlas of the mice brains using the FMRIB Software Library linear registration program FLIRT. The atlas was then transformed back to each individual data set with the registration matrices from Advanced Normalization Tools. To generate parametric T1 maps, multi-TR images were fit to the equation $S_{TR} = S_0(1 - e^{-TR/T1})$ using nonlinear regression in ImageJ. From T1 maps, the T1 relaxation rate (R1 in ms^{-1}) is calculated and exported from regions of interest.

Statistics

For all experiments, both sexes of mice were included. Data are presented as means \pm SD. Significance was assessed by Student's *t* test for single comparisons and by ANOVA/Tukey's test for multiple comparisons. Statistical significance was set at $P < 0.05$. Analyses were performed using GraphPad Prism.

RESULTS

Deletion of Intestinal *Zip14* Causes Impaired Serosal-to-Mucosal ^{54}Mn Transport

A representative PCR amplification for genotyping was shown in Fig. 1A. Intestine-specific ablation of *Zip14* was confirmed by Western blotting of ZIP14 protein. Tissues from both villin-cre (VC) and fl/fl mice were included as controls. ZIP14 was deleted only in the intestine of the I-KO mice (Fig. 1B). Western blotting shows expression of ZIP14 between I-KO and WB-KO mice (Fig. 1C). Absence of ZIP14 from only the intestine of the I-KO mice confirms tissue specificity. To determine the role of intestinal ZIP14 in Mn clearance, we conducted ^{54}Mn -uptake studies using I-KO mice to ascertain the direction of Mn transport mediated by ZIP14. ^{54}Mn was administered via 2 routes, and radioactivity in the intestine was measured. There was no difference in the amount of radioac-

tivity in the intestine of I-KO, VC, and fl/fl mice when ^{54}Mn was administered via oral gavage (Fig. 1D), indicating that intestinal ^{54}Mn absorption was not affected by ZIP14 deficiency. However, significantly ($P < 0.001$) less radioactivity was detected in the intestine of *Zip14* I-KO mice when ^{54}Mn was administered via subcutaneous injection, indicating that the intestine-specific deletion of *Zip14* decreased serosal-to-mucosal transcellular Mn transport. In the following experiments, fl/fl mice were used as controls because we confirmed that there was no difference in ^{54}Mn uptake between fl/fl and VC mice (Fig. 1D).

Deletion of Intestinal *Zip14* Leads to Systemic and Brain Mn Accumulation

To test whether impaired intestinal ZIP14-mediated Mn excretion affects systemic Mn metabolism, we compared systemic ^{54}Mn distribution between WB-KO and I-KO mice. Our results revealed that when it was given via subcutaneous injection, the amount of ^{54}Mn was significantly less in the intestines of both WB-KO and I-KO mice (Fig. 2A). Furthermore, the amount of ^{54}Mn was significantly greater in the blood and brain of the WB and I-KO mice compared with their controls (Fig. 2B). The magnitude of increase in ^{54}Mn was less in I-KO mice compared with WB-KO mice.

The key route of Mn elimination is through the hepatobiliary system. To evaluate the hepatobiliary clearance of Mn, we measured liver ^{54}Mn uptake. Of note, ^{54}Mn uptake was impaired in WB-KO and enhanced in I-KO, suggesting that a lack of intestinal ZIP14 was compensated for in the I-KO mice through increased Mn elimination via the hepatobiliary system (Fig. 2C). Furthermore, ^{54}Mn uptake was not different between kidney and pancreas of fl/fl and I-KO

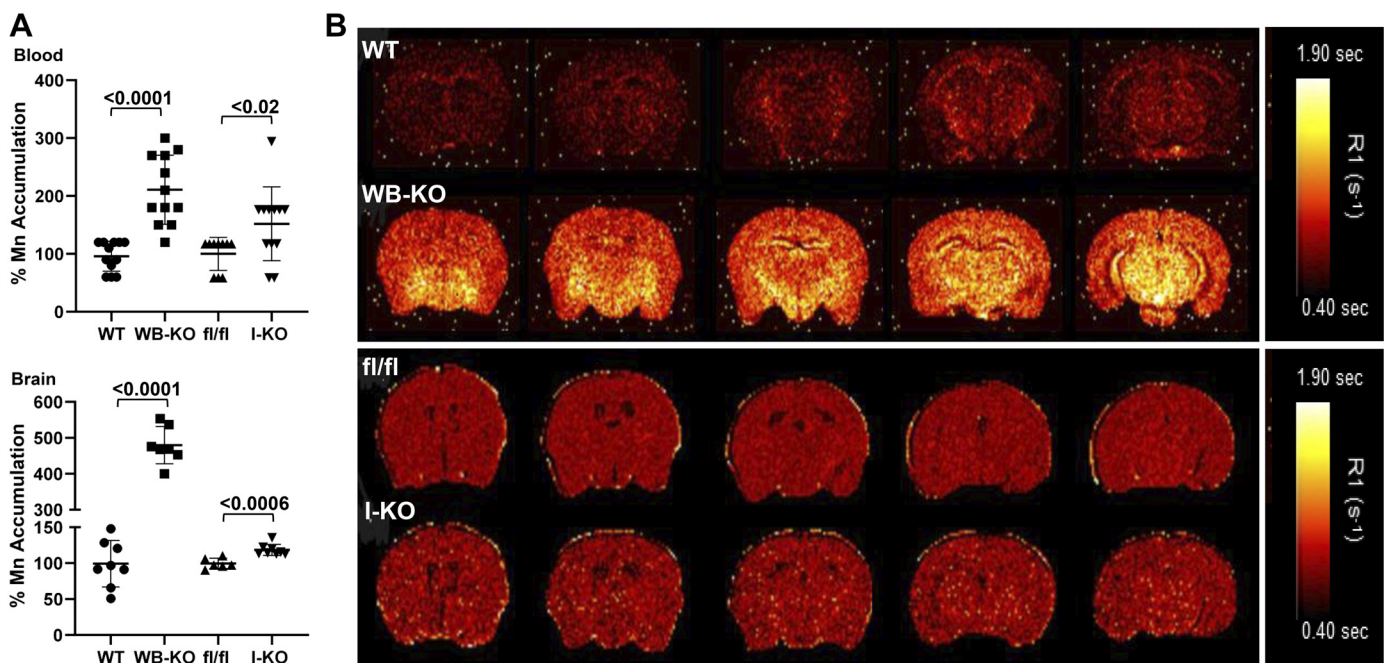


Fig. 3. Deletion of intestinal *Zip14* leads to manganese in mice. **A**: Mn concentrations in blood and brain were measured by Microwave Plasma-Atomic Emission Spectrometer. **B**: Representative magnetic resonance images with a quantitative map of R1 relaxation rates (inverse of T1 values). Values are reported as means \pm SD; $n = 7-14$ (both female and male mice were included). Student's *t* test for wild-type (WT) vs. whole body *Zip14* knockout (WB-KO) and floxed *Zip14* (fl/fl) vs. intestine-specific *Zip14* knockout (I-KO) comparison.

mice, whereas ^{54}Mn uptake was higher and lower in pancreas and kidney of WB-KO mice, respectively, suggesting that ZIP14 might be involved with ^{54}Mn uptake in the kidney (Fig. 2D).

Next, to evaluate the influence of intestinal ZIP14 on brain Mn, we measured Mn accumulation using MP-AES. The Mn concentration was greater in the blood and brain of both the WB-KO and I-KO mice compared with their controls (Fig. 3A). As expected, relative accumulation was less in the I-KO mice. Furthermore, we used MRI analysis to evaluate brain Mn accumulation between WB-KO and I-KO mice. Signal intensity was greater in the brains of I-KO mice when compared with fl/fl mice. Similar to ^{54}Mn uptake and MP-AES data, the differences in MRI signal intensity between the brains of the fl/fl and I-KO mice were less than those between the WB-KO and WT mice (Fig. 3B). Nevertheless, the images from the I-KO mice clearly show punctate regions of increased intensity consistent with Mn accumulation. Of note, the MRI images, which were obtained without any enhancement, reflected endogenous Mn in brains of both genotypes and were from young adult mice maintained under barrier conditions with normal husbandry. These data collectively suggest that deletion of intestinal *Zip14* was sufficient to cause systemic Mn overload

and that intestinal ZIP14 is a significant contributor to Mn homeostasis.

Neuroinflammation and Motor Dysfunction in Intestine-Specific *Zip14* KO Is Amplified with High Mn Exposure

Deletion of intestinal *Zip14* caused systemic and brain Mn overload; however, the magnitude of increases was less in I-KO mice compared with WB-KO mice. Therefore, we have conducted Mn supplementation studies with I-KO mice to increase exposure. Deletion of intestinal ZIP14 was confirmed by Western blot (Fig. 4A). Following Mn exposure, increased intestinal Mn concentrations were found in the fl/fl mice but were not observed in the I-KO mice (Fig. 4A). Moreover, the Mn concentration of luminal and fecal content of Mn-supplemented I-KO mice was significantly less than that in Mn-supplemented fl/fl mice (Fig. 4B). Mn concentrations were greater in the livers of the I-KO mice compared with the fl/fl mice in the control group, demonstrating that greater hepatic Mn clearance occurs when hepatic ZIP14 is functional but intestinal ZIP14 is not functional (Fig. 4C).

Mn is neurotoxic; thus, we next measured the blood and brain Mn concentrations. Mn concentrations were greater in

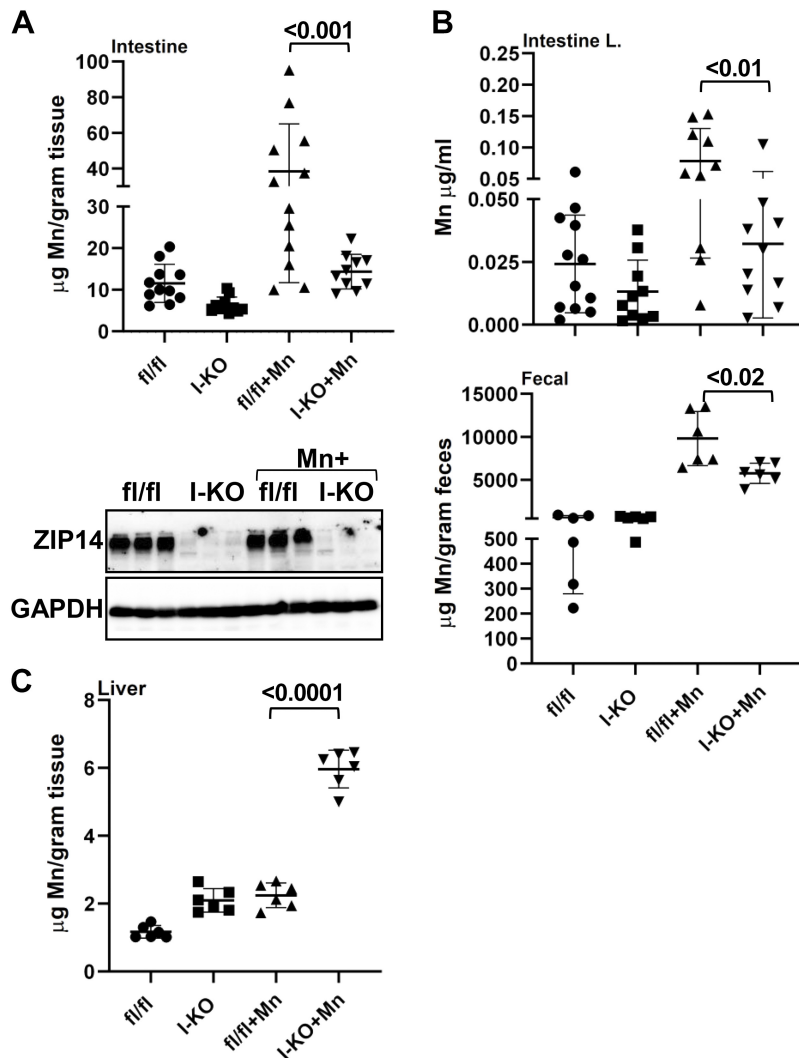


Fig. 4. Comparison of Mn concentration between control and Mn-supplemented intestine-specific *Zip14* knockout (I-KO). Representative Western blot images showing the absence of ZIP14 in I-KO intestines (A). Mn concentrations in the intestine (A), intestine luminal and fecal content (B), and liver (C) were measured by Microwave Plasma-Atomic Emission Spectrometer. Values are means \pm SD; $n = 6-12$ (both female and male mice were included). Significance was assessed by one-way ANOVA. fl/fl, floxed *Zip14*.

blood and brain of I-KO mice compared with fl/fl mice in the control group (Fig. 5, A and B). Mn concentrations in Mn-supplemented fl/fl mice were comparable with those in the I-KO unsupplemented mice. Mn supplementation further enhanced the Mn accumulation in blood and brains of I-KO mice compared with the Mn-supplemented fl/fl mice, however. Importantly, there was no change between groups in brain Zn and Fe concentrations (Fig. 5C). Importantly, the Mn-supplemented I-KO group had the greatest increase in Mn concentrations, further confirming that impaired Mn excretion in I-KO mice occurs via the intestine.

To test the physiological consequences of Mn overload, we assessed motor functions using the inverted grip, balance beam traversal, pole descent test, and fecal output methods. The Mn-supplemented I-KO mice required significantly more time to cross a balance beam compared with fl/fl control mice (Fig. 6A), whereas there was no difference in the time to descend a pole (data not shown). Furthermore, the total output of fecal pellets was significantly lower in Mn-supplemented I-KO mice (Fig. 6A). We found no difference in body weight and limb strength (inverted grid assay) (data not shown). These data collectively showed that at the end of 1 mo of chronic Mn exposure, I-KO mice developed initial indices of motor dysfunction; however, the whole spectrum of manganese had not been obtained.

To investigate the biochemical and physiological underpinnings of Mn-induced motor dysfunction, we measured reactive

oxygen species (ROS) and cytokine expressions in whole brain lysates. Our results revealed an increased amount of ROS in the I-KO and Mn-supplemented fl/fl mice compared with the fl/fl mice (Fig. 6B). The highest increase was found in Mn-supplemented I-KO mice; however, the difference was not statistically significant ($P = 0.07$). Similarly, the highest increase for *Il6* mRNA was found in Mn-supplemented I-KO mice; the difference was also not statistically significant ($P = 0.07$) (Fig. 6C). However, the expression of inducible nitric oxide synthase and *TNF α* mRNAs was significantly increased in Mn-supplemented I-KO mice when compared with control fl/fl mice (Fig. 6C). These varying levels of increases in ROS and cytokine levels supporting the previous observation in which I-KO mice developed only initial indices of motor dysfunction following 1 mo of chronic Mn exposure (Fig. 6A).

DISCUSSION

In the present study, using whole body and intestine-specific *Zip14* KO mice, we demonstrate that intestinal ZIP14 is essential for Mn homeostasis. Mice with a deletion of intestinal *Zip14* displayed a phenotype that included impaired serosal-to-mucosal Mn transport, resulting in increased liver, blood, and brain Mn accumulation. Mn supplementation greatly enhanced the brain Mn overload in I-KO mice, which showed early parkinsonism symptoms.

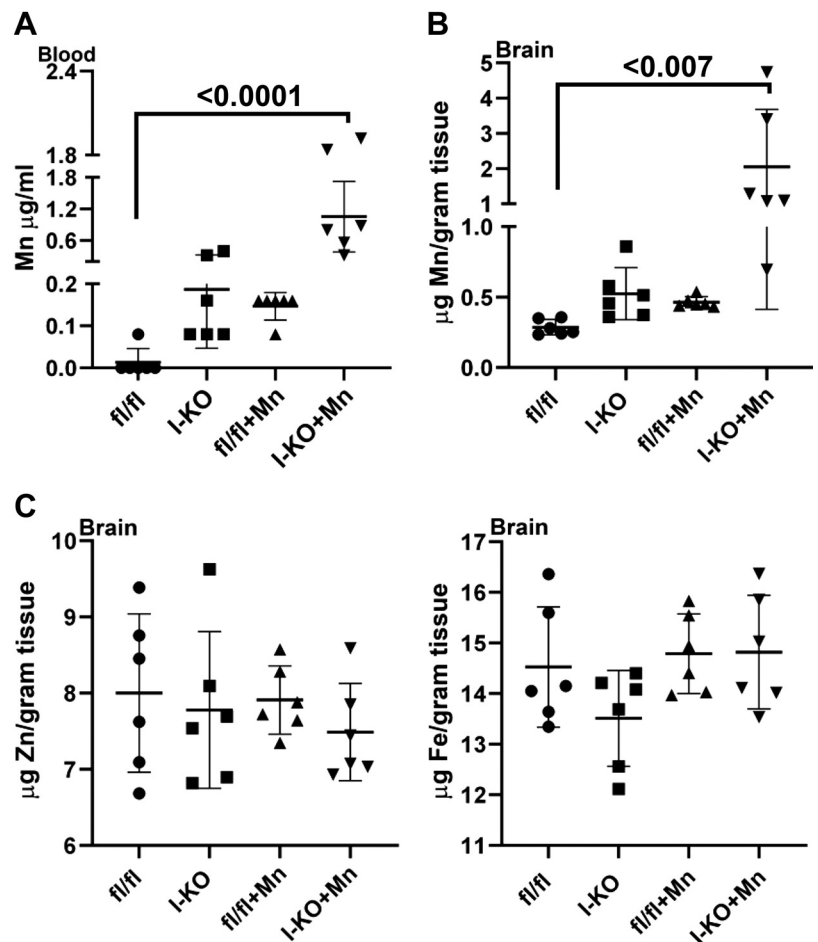


Fig. 5. Comparison of metal concentrations between control and Mn-supplemented intestine-specific *Zip14* knockout (I-KO). Mn concentrations in blood (A) and brain (B) and Zn and Fe concentrations in the brain (C) were measured by Microwave Plasma-Atomic Emission Spectrometer. Values are means \pm SD; $n = 6$ (both female and male mice were included). Significance was assessed by one-way ANOVA. fl/fl, floxed *Zip14*.

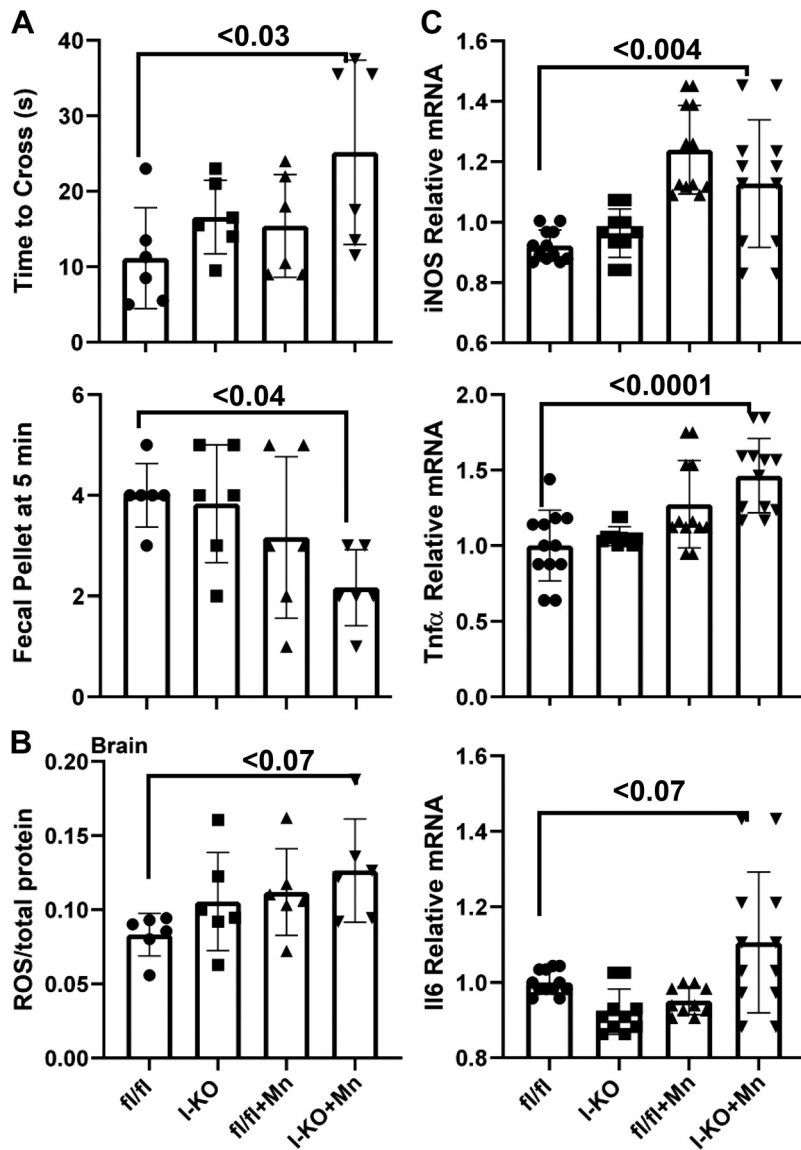


Fig. 6. Comparison of motor functions between control and Mn-supplemented intestine-specific *Zip14* knockout (I-KO) mice. Time to cross the balance beam and fecal output were counted (A). Reactive oxygen species (ROS) (B) and cytokine expressions (C) were measured. Values are means \pm SD; $n = 6$ (both female and male mice were included). Significance was assessed by one-way ANOVA. fl/fl, floxed *Zip14*; iNOS, inducible nitric oxide synthase.

Manganese metabolism is homeostatically maintained through limited absorption by the small intestine, with elimination occurring via hepatobiliary, pancreatic, and urinary (minimally) excretions (7). The plethora of transporters with proposed roles in manganese metabolism has been documented (15). The list includes divalent metal transporter 1, transferrin receptor, calcium channels, Park9/ATP13A2, $\text{Na}^+/\text{Ca}^{2+}$ exchanger, SPCA1, and ferroportin. However, the precise molecular mechanisms that underlie Mn homeostasis are poorly understood. ZIP14/SLC39A14 is a ZIP family transmembrane protein that regulates intracellular levels of Zn, Mn, and Fe. Although occupational and environmental Mn exposures are known sources of Mn toxicity, genetic mutations in metal transporters, including ZIP14, also cause Mn-induced parkinsonism. Mutations in the *SLC39A14* gene encoding the ZIP14 transporter were found in patients with childhood-onset parkinsonism and dystonia with systemic and brain Mn accumulation (35). Deletion of *Zip14* expression in zebrafish recapitulated the human brain Mn accumulation phenotype of ZIP14 mutation carriers (35). However, Mn concentration in the

abdominal viscera of WT and mutant zebrafish was not different. Using whole body *Zip14*-KO mice, we have previously shown that WB *Zip14*-KO mice displayed phenotypes similar to those of human carriers of ZIP14 mutations, including spontaneous systemic and brain Mn overload with motor dysfunction and impaired hepatic Mn uptake (3). Our findings with *Zip14*-KO mice were confirmed by 2 independent research groups (16, 37), collectively supporting the use of *Zip14*-KO mouse models as a relevant model system with which to further investigate the organ/tissue-specific role of ZIP14-mediated Mn transport in Mn homeostasis.

The early studies with ^{54}Mn revealed that hepatobiliary system was a major route for Mn elimination from the body (5). However, using liver-specific *Zip14*-KO mice, Xin et al. (37) showed that there was no Mn accumulation in the brain or other tissues of liver-specific *Zip14*-KO mice, which have considerably lower hepatic Mn levels. This finding supports our hypothesis that there are other highly efficient Mn elimination routes in the body. We previously showed that ZIP14 is localized at the basolateral site of the enterocytes (3, 14).

Furthermore, intestinal Mn elimination was impaired in WB *Zip14*-KO mice. Therefore we generated I-KO mice to explore the specific role of intestinal *Zip14* in Mn elimination/detoxification. We found that Mn transport in the serosal-to-mucosal direction was impaired and, importantly, that Mn accumulated in the blood and brain at steady state. This novel finding suggests that deletion of intestinal *Zip14* is sufficient to cause systemic Mn overload and that intestinal ZIP14 is a significant contributor to Mn homeostasis.

The known Mn elimination routes are hepatobiliary (major), pancreatic, and urinary (minimally) excretion (7). Therefore, we compared ^{54}Mn transport in these tissues of WB-KO and I-KO mice. Pancreatic ^{54}Mn uptake was impaired, and ^{54}Mn uptake by kidney was enhanced in WB *Zip14*-KO mice. In contrast, we have not observed any changes in pancreas and kidney of I-KO mice compared with fl/fl control mice. However, there was a significant increase in the liver ^{54}Mn uptake and Mn accumulation. This suggests that there is an activation of a hepatic compensation mechanism. These novel differences in tissue ^{54}Mn uptake and Mn accumulation in I-KO mice are providing new aspects for the paths of systemic Mn detoxification.

Impaired manganese (Mn) homeostasis results in excess Mn and neurotoxicity; however, the underlying molecular mechanisms have not been clearly defined. It has been suggested that oxidative stress and associated neuroinflammation lead to neurodegeneration and parkinsonism (motor dysfunction) (26, 27, 30, 32). Our results revealed that ROS and cytokine expressions were highly upregulated in the brain of Mn-supplemented I-KO mice. Notably, only Mn (but not zinc or iron) levels in the brains of I-KO and Mn-supplemented mice were greater, providing evidence for the specific effect of Mn on neuroinflammation. The main site of Mn-induced inflammation in the brain remains to be elucidated.

In conclusion, we show here the role of intestinal ZIP14 on Mn elimination and homeostasis at the organism level. Mn elimination by intestinal ZIP14 is essential to maintain Mn homeostasis because the hepatic compensation mechanism is not sufficient to prevent Mn overload and subsequent neurotoxicity.

ACKNOWLEDGEMENTS

The authors acknowledge the support from the National High Magnetic Field Laboratory's Advanced Magnetic Resonance Imaging and Spectroscopy Facility (National Science Foundation Cooperative Agreement no. DMR-1157490 and the state of Florida). Graphical abstract was prepared by Allison A. Stevens, AASarts.com.

GRANTS

This project was supported by the National Institute of Diabetes and Digestive and Kidney Diseases Grant 5R01-DK-094244 to R. J. Cousins and Cornell University Division of Nutritional Sciences funds to T. B. Aydemir.

DISCLOSURES

No conflicts of interest, financial or otherwise, are declared by the author(s).

AUTHOR CONTRIBUTIONS

T.B.A. and R.J.C. conceived and designed research; T.B.A., T.L.T., C.H.R., and M.P. performed experiments; T.B.A., T.L.T., M.F., and R.J.C. analyzed data; T.B.A., T.L.T., M.F., and R.J.C. interpreted results of experiments; T.B.A. and M.F. prepared figures; T.B.A. and R.J.C. drafted manuscript; T.B.A., M.F., and R.J.C. edited and revised manuscript; T.B.A., T.L.T., C.H.R., M.P., M.F., and R.J.C. approved final version of manuscript.

REFERENCES

1. **Aboud AA, Tidball AM, Kumar KK, Neely MD, Ess KC, Erikson KM, Bowman AB.** Genetic risk for Parkinson's disease correlates with alterations in neuronal manganese sensitivity between two human subjects. *Neurotoxicology* 33: 1443–1449, 2012. doi:10.1016/j.neuro.2012.10.009.
2. **Aydemir TB, Chang S-M, Guthrie GJ, Maki AB, Ryu M-S, Karabiyik A, Cousins RJ.** Zinc transporter ZIP14 functions in hepatic zinc, iron and glucose homeostasis during the innate immune response (endotoxemia). *PLoS One* 7: e48679, 2012. doi:10.1371/journal.pone.0048679.
3. **Aydemir TB, Kim M-H, Kim J, Colon-Perez LM, Banan G, Mareci TH, Febo M, Cousins RJ.** Metal transporter *Zip14* (*Slc39a14*) deletion in mice increases manganese deposition and produces neurotoxic signatures and diminished motor activity. *J Neurosci* 37: 5996–6006, 2017. doi:10.1523/JNEUROSCI.0285-17.2017.
4. **Aydemir TB, Sitren HS, Cousins RJ.** The zinc transporter *Zip14* influences c-Met phosphorylation and hepatocyte proliferation during liver regeneration in mice. *Gastroenterology* 142: 1536–1546.e5, 2012. doi:10.1053/j.gastro.2012.02.046.
5. **Bertinchamps AJ, Miller ST, Cotzias GC.** Interdependence of routes excreting manganese. *Am J Physiol* 211: 217–224, 1966. doi:10.1152/ajplegacy.1966.211.1.217.
6. **Boycott KM, Beaulieu CL, Kernohan KD, Gebril OH, Mhanni A, Chudley AE, Redl D, Qin W, Hampson S, Küry S, Tetreault M, Puffenberger EG, Scott JN, Bezieau S, Reis A, Uebe S, Schumacher J, Hegele RA, McLeod DR, Gálvez-Peralta M, Majewski J, Ramaekers VT, Nebert DW, Innes AM, Parboosingh JS, Abou Jamra R; Care4Rare Canada Consortium.** Autosomal-recessive intellectual disability with cerebellar atrophy syndrome caused by mutation of the manganese and zinc transporter gene SLC39A8. *Am J Hum Genet* 97: 886–893, 2015. doi:10.1016/j.ajhg.2015.11.002.
7. **Buchman AL.** *Modern Nutrition in Health and Disease* (11th ed.). Philadelphia, PA: Wolters Kluwer Health/Lippincott Williams & Wilkins, 2014, p. 238–244.
8. **Carmona A, Roudeau S, Perrin L, Veronesi G, Ortega R.** Environmental manganese compounds accumulate as Mn(II) within the Golgi apparatus of dopamine cells: relationship between speciation, subcellular distribution, and cytotoxicity. *Metallomics* 6: 822–832, 2014. doi:10.1039/c4mt00012a.
9. **Caudle WM.** Occupational metal exposure and parkinsonism. In: *Neurotoxicity of Metals*. 2017. doi:10.1007/978-3-319-60189-2_7.
10. **Chen P, Bornhorst J, Aschner M.** Manganese metabolism in humans. *Front Biosci* 23: 1655–1679, 2018. doi:10.2741/4665.
11. **Chen P, Miah MR, Aschner M.** Metals and neurodegeneration. *F1000 Res* 5: 366, 2016. doi:10.12688/f1000research.7431.1.
12. **Freeland-Graves JH, Mousa TY, Kim S.** International variability in diet and requirements of manganese: Causes and consequences. *J Trace Elem Med Biol* 38: 24–32, 2016. doi:10.1016/j.jtemb.2016.05.004.
13. **Guilarte TR, Gonzales KK.** Manganese-induced Parkinsonism is not idiopathic Parkinson's Disease: environmental and genetic evidence. *Toxicol Sci* 146: 204–212, 2015. doi:10.1093/toxsci/kfv099.
14. **Guthrie GJ, Aydemir TB, Troche C, Martin AB, Chang S-M, Cousins RJ.** Influence of ZIP14 (*slc39a14*) on intestinal zinc processing and barrier function. *Am J Physiol Gastrointest Liver Physiol* 308: G171–G178, 2015. doi:10.1152/ajpgi.00021.2014.
15. **Horning KJ, Caito SW, Tipps KG, Bowman AB, Aschner M.** Manganese is essential for neuronal health. *Annu Rev Nutr* 35: 71–108, 2015. doi:10.1146/annurev-nutr-071714-034419.
16. **Jenkitkasemwong S, Akinyode A, Paulus E, Weiskirchen R, Hojyo S, Fukada T, Giraldo G, Schrier J, Garcia A, Janus C, Giasson B, Knutson MD.** SLC39A14 deficiency alters manganese homeostasis and excretion resulting in brain manganese accumulation and motor deficits in mice. *Proc Natl Acad Sci USA* 115: E1769–E1778, 2018. doi:10.1073/pnas.1720739115.
17. **Juneja M, Shamim U, Joshi A, Mathur A, Uppili B, Sairam S, Ambawat S, Dixit R, Faruq M.** A novel mutation in SLC39A14 causing hypermanganesemia associated with infantile onset dystonia. *J Gene Med* 20: e3012, 2018. doi:10.1002/jgm.3012.
18. **Kwakye GF, Paoliello MMB, Mukhopadhyay S, Bowman AB, Aschner M.** Manganese-induced Parkinsonism and Parkinson's disease: shared and distinguishable features. *Int J Environ Res Public Health* 12: 7519–7540, 2015. doi:10.3390/ijerph120707519.

19. Leyva-Illades D, Chen P, Zogzas CE, Hutchens S, Mercado JM, Swaim CD, Morrisett RA, Bowman AB, Aschner M, Mukhopadhyay S. SLC30A10 is a cell surface-localized manganese efflux transporter, and parkinsonism-causing mutations block its intracellular trafficking and efflux activity. *J Neurosci* 34: 14079–14095, 2014. doi:10.1523/JNEUROSCI.2329-14.2014.
20. Lin W, Vann DR, Doulias P-T, Wang T, Landesberg G, Li X, Ricciotti E, Scalia R, He M, Hand NJ, Rader DJ. Hepatic metal ion transporter ZIP8 regulates manganese homeostasis and manganese-dependent enzyme activity. *J Clin Invest* 127: 2407–2417, 2017. doi:10.1172/JCI90896.
21. Liuzzi JP, Aydemir F, Nam H, Knutson MD, Cousins RJ. Zip14 (Slc39a14) mediates non-transferrin-bound iron uptake into cells. *Proc Natl Acad Sci USA* 103: 13612–13617, 2006. doi:10.1073/pnas.0606424103.
22. Lucchini RG, Aschner M, Landrigan PJ, Cranmer JM. Neurotoxicity of manganese: Indications for future research and public health intervention from the Manganese 2016 conference. *Neurotoxicology* 64: 1–4, 2018. doi:10.1016/j.neuro.2018.01.002.
23. Marti-Sanchez L, Ortigoza-Escobar JD, Darling A, Villaronga M, Baide H, Molero-Luis M, Battlori M, Vanegas MI, Muchart J, Aquino L, Artuch R, Macaya A, Kurian MA, Dueñas P. Hypermanganesemia due to mutations in SLC39A14: further insights into Mn deposition in the central nervous system. *Orphanet J Rare Dis* 13: 28, 2018. doi:10.1186/s13023-018-0758-x.
24. O'Neal SL, Zheng W. Manganese toxicity upon overexposure: a decade in review. *Curr Environ Health Rep* 2: 315–328, 2015. doi:10.1007/s40572-015-0056-x.
25. Park JH, Högrefe M, Grüneberg M, DuChesne I, von der Heiden AL, Reunert J, Schlingmann KP, Boycott KM, Beaulieu CL, Mhanni AA, Innes AM, Hörtnagel K, Biskup S, Gleixner EM, Kurlemann G, Fiedler B, Omran H, Rutsch F, Wada Y, Tsiakas K, Santer R, Nebert DW, Rust S, Marquardt T. SLC39A8 deficiency: a disorder of manganese transport and glycosylation. *Am J Hum Genet* 97: 894–903, 2015. doi:10.1016/j.ajhg.2015.11.003.
26. Peres TV, Schettinger MRC, Chen P, Carvalho F, Avila DS, Bowman AB, Aschner M. Manganese-induced neurotoxicity: a review of its behavioral consequences and neuroprotective strategies. *BMC Pharmacol Toxicol* 17: 57, 2016. doi:10.1186/s40360-016-0099-0.
27. Pfalzer AC, Bowman AB. Relationships between essential manganese biology and manganese toxicity in neurological disease. *Curr Environ Health Rep* 4: 223–228, 2017. doi:10.1007/s40572-017-0136-1.
28. Quadri M, Federico A, Zhao T, Breedveld GJ, Battisti C, Delnooz C, Severijnen LA, Di Toro Mammarella L, Mignarri A, Monti L, Sanna A, Lu P, Punzo F, Cossu G, Willemsen R, Rasi F, Oostra BA, van de Warrenburg BP, Bonifati V. Mutations in SLC30A10 cause parkinsonism and dystonia with hypermanganesemia, polycythemia, and chronic liver disease. *Am J Hum Genet* 90: 467–477, 2012. doi:10.1016/j.ajhg.2012.01.017.
29. Racette BA. Manganism in the 21st century: the Hanninen lecture. *Neurotoxicology* 45: 201–207, 2014. doi:10.1016/j.neuro.2013.09.007.
30. Racette BA, Aschner M, Guilarte TR, Dydak U, Criswell SR, Zheng W. Pathophysiology of manganese-associated neurotoxicity. *Neurotoxicology* 33: 881–886, 2012. doi:10.1016/j.neuro.2011.12.010.
31. Rodan LH, Hauptman M, D'Gama AM, Qualls AE, Cao S, Tuschl K, Al-Jasmi F, Hertecant J, Hayflick SJ, Wessling-Resnick M, Yang ET, Berry GT, Gropman A, Woolf AD, Agrawal PB. Novel founder intronic variant in SLC39A14 in two families causing Manganism and potential treatment strategies. *Mol Genet Metab* 124: 161–167, 2018. doi:10.1016/j.ymgme.2018.04.002.
32. Roth JA. Mutual neurotoxic mechanisms controlling manganese and parkinsonism. In: *Manganese in Health and Disease*. 2014. doi:10.1039/9781782622383-00221.
33. Truett GE, Heeger P, Mynatt RL, Truett AA, Walker JA, Warman ML. Preparation of PCR-quality mouse genomic DNA with hot sodium hydroxide and tris (HotSHOT). *Biotechniques* 29: 52–54, 2000. doi:10.2144/00291bm09.
34. Tuschl K, Clayton PT, Gospe SM Jr, Gulab S, Ibrahim S, Singhi P, Aulakh R, Ribeiro RT, Barsottini OG, Zaki MS, Del Rosario ML, Dyack S, Price V, Rideout A, Gordon K, Wevers RA, Chong WK, Mills PB. Syndrome of hepatic cirrhosis, dystonia, polycythemia, and hypermanganesemia caused by mutations in SLC30A10, a manganese transporter in man. *Am J Hum Genet* 90: 457–466, 2012. doi:10.1016/j.ajhg.2012.01.018.
35. Tuschl K, Meyer E, Valdivia LE, Zhao N, Dadswell C, Abdul-Sada A, Hung CY, Simpson MA, Chong WK, Jacques TS, Woltjer RL, Eaton S, Gregory A, Sanford L, Kara E, Houlden H, Cuno SM, Prokisch H, Valletta L, Tiranti V, Younis R, Maher ER, Spencer J, Straatman-Iwanowska A, Gissen P, Selim LA, Pintos-Morell G, Coroleu-Lletget W, Mohammad SS, Yoganathan S, Dale RC, Thomas M, Rihel J, Bodamer OA, Enns CA, Hayflick SJ, Clayton PT, Mills PB, Kurian MA, Wilson SW. Mutations in SLC39A14 disrupt manganese homeostasis and cause childhood-onset parkinsonism-dystonia. *Nat Commun* 7: 11601, 2016. doi:10.1038/ncomms11601.
36. Wasserman GA, Liu X, Parvez F, Ahsan H, Levy D, Factor-Litvak P, Kline J, van Geen A, Slavkovich V, LoIacono NJ, Cheng Z, Zheng Y, Graziano JH. Water manganese exposure and children's intellectual function in Arahazar, Bangladesh. *Environ Health Perspect* 114: 124–129, 2006. doi:10.1289/ehp.8030.
37. Xin Y, Gao H, Wang J, Qiang Y, Imam MU, Li Y, Wang J, Zhang R, Zhang H, Yu Y, Wang H, Luo H, Shi C, Xu Y, Hojyo S, Fukada T, Min J, Wang F. Manganese transporter Slc39a14 deficiency revealed its key role in maintaining manganese homeostasis in mice. *Cell Discov* 3: 17025, 2017. doi:10.1038/celldisc.2017.25.
38. Zeglami A, Abugrara A, Kabuka M. Autosomal-recessive iron deficiency anemia, dystonia and hypermanganesemia caused by new variant mutation of the manganese transporter gene SLC39A14. *Acta Neurologica Belgica* 119: 379–384, 2019. doi:10.1007/s13760-018-1024-7.